Supplementary Material

for "Coherent turbulent structures in a rapid contraction"

by Alhareth, Mugundhan, Langley & Thoroddsen

S1. Curve fitting of the alignment PDFs

The alignment PDFs are strongly peaked around the streamwise direction, where $\theta = 0$. To quantify the shape of the PDF of $|cos\theta|$, we fit its peak near the streamwise alignment with an inverted fifth-order polynomial in terms of $\phi = 1 - |cos\theta|$, as seen in Figure S1. This fit works well for the full range [0,1]. The fits are of the form,

$$PDF = \frac{1}{\phi^5 + a_1\phi^4 + a_2\phi^3 + a_3\phi^2 + a_4\phi + + a_5}. \tag{S1.1}$$

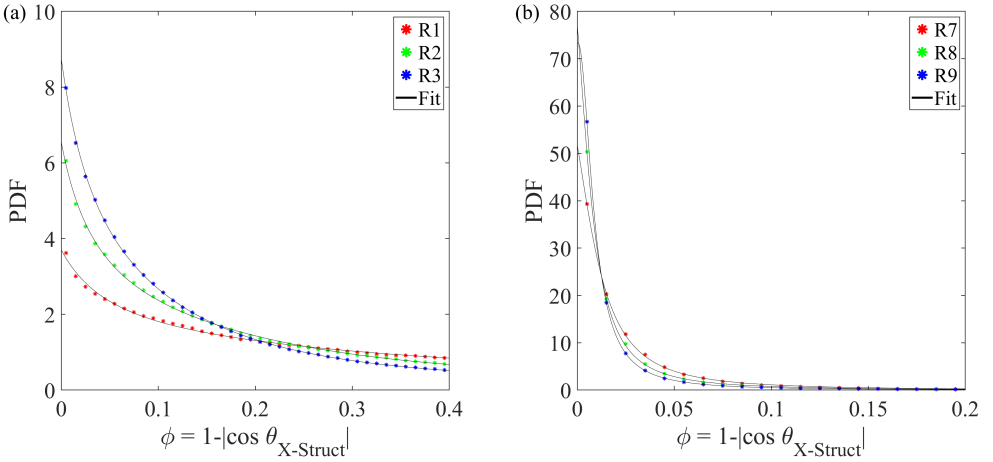

FIGURE S1. The alignment PDFs and the inverted fifth-order polynomial fits obtained in volume sub-regions (a) R1-R3 inside region P1 near the inlet to the contraction; and (b) R7-R9 inside region P3 towards the exit of the contraction. See main Figure 1(b) for precise locations. These PDFs are computed using 100 bins spanning the range [0,1]. The cumulative probability of 99.5% is reached before the fit reaches the last data point and thereby relies on the near-perfect interpolation of the fit. Thereby the computation of the probability does not involve the value of fit at $\phi = 0$, where the extrapolation is uncertain.

S2. Volume of coherent vortical structures

To ascertain the prevalence of the coherent vortical structures, we have calculated their volumes, using thresholding on the absolute value of the vorticity magnitude $|\boldsymbol{\omega}|$= 40 s^{-1}. Figure S2 shows the morphology of the vortical structures which encompass the largest measured volume fractions.

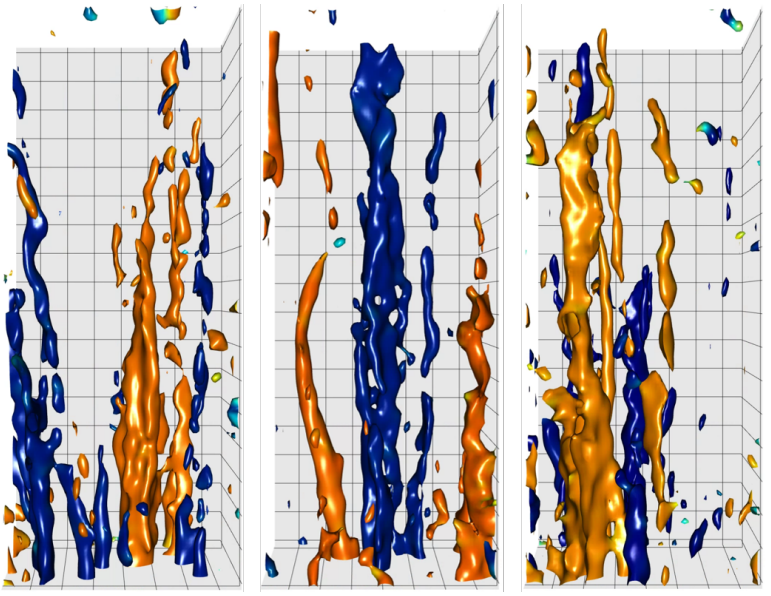

FIGURE S2. The instantaneous coherent structures corresponding to the largest peak volume fractions marked by red dots in Figure 8(a). Using thresholding of $|\boldsymbol{\omega}|$= 40 s^{-1}, corresponding to $|\omega|/S_{\max}$ = 0.78.

S3. Choice of a threshold value for vorticity magnitude criterion

Figure S3 shows how we select the threshold value for the prominent coherent streamwise vortical structure in region P3, near the exit of the contraction. We compare the shapes for isosurfaces over a range of $|\omega|$ = 20−50 s^{-1}, while only visualizing structures having a volume greater than 100 voxels. For the lowest threshold value of 20 s^{-1} the isosurfaces fill most of the volume, with irregular shapes. The primary coherent structure is still visible, but random tendrils emerge from it and are not coherent in time. This makes it difficult to identify distinct and dominant structures. At 30 s^{-1} the structure is more defined and regular, while numerous more discontinuous smaller structures persist. On the other hand, for the highest threshold value of $|\omega|$ =50 s^{-1} the vortex core breaks up, especially at the inlet, where it has not stretched as much as at the outlet. This makes it hard to identify and track with time. To isolate the coherent structures we thus arrive at an intermediate cut-off value of $|\omega|$ =40 s^{-1}.

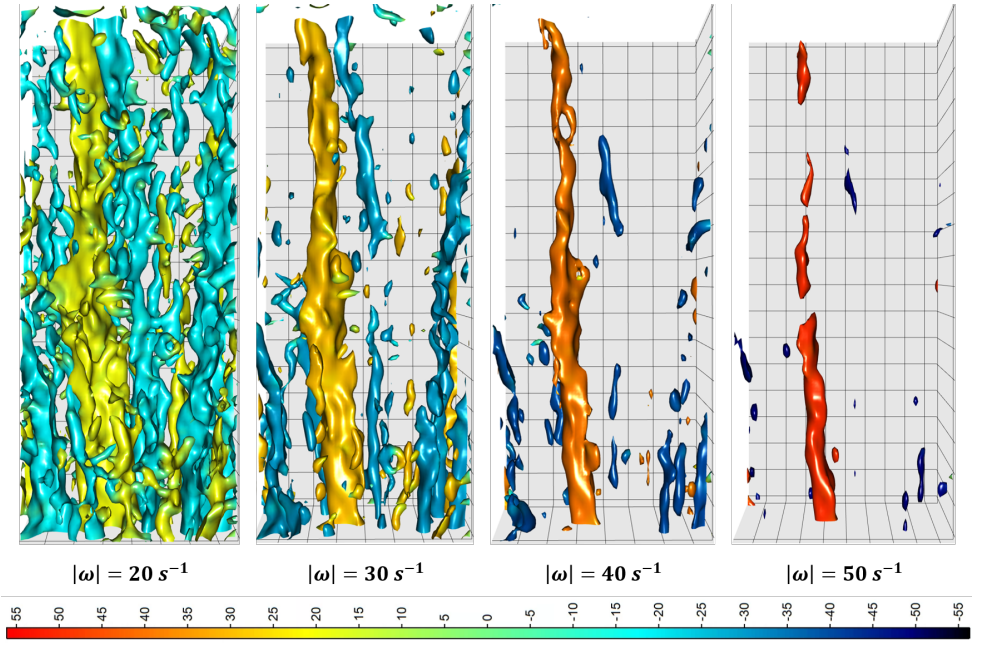

FIGURE S3. Coherent vortical structures visualized with different isosurface thresholds corresponding to $|\omega|$ = 20−50 s^{-1} ($|\omega|/S_{max}$ = 0.63−1.56) at the same instant in region P3. The isosurfaces are colored by ω_x whose color bar is shown.

S4. Fitting of coherent structures

We use the *watershed* algorithm in MATLAB to identify and tag the coherent structures visualized by isosurface of $|\omega|$ and also filtered based on the volume occupied by the structure. The geometric properties of the tagged structures are extracted using the *regionprops3* function in MATLAB. The function fits an equivalent ellipsoid which has the same normalized central moments as the structure. We use the major axis of this ellipsoid to characterize the alignment and length of the structures. Figure S4 shows three examples of the longest, instantaneous structures identified in region P3, together with the centroid and major axis of the equivalent ellipsoid.

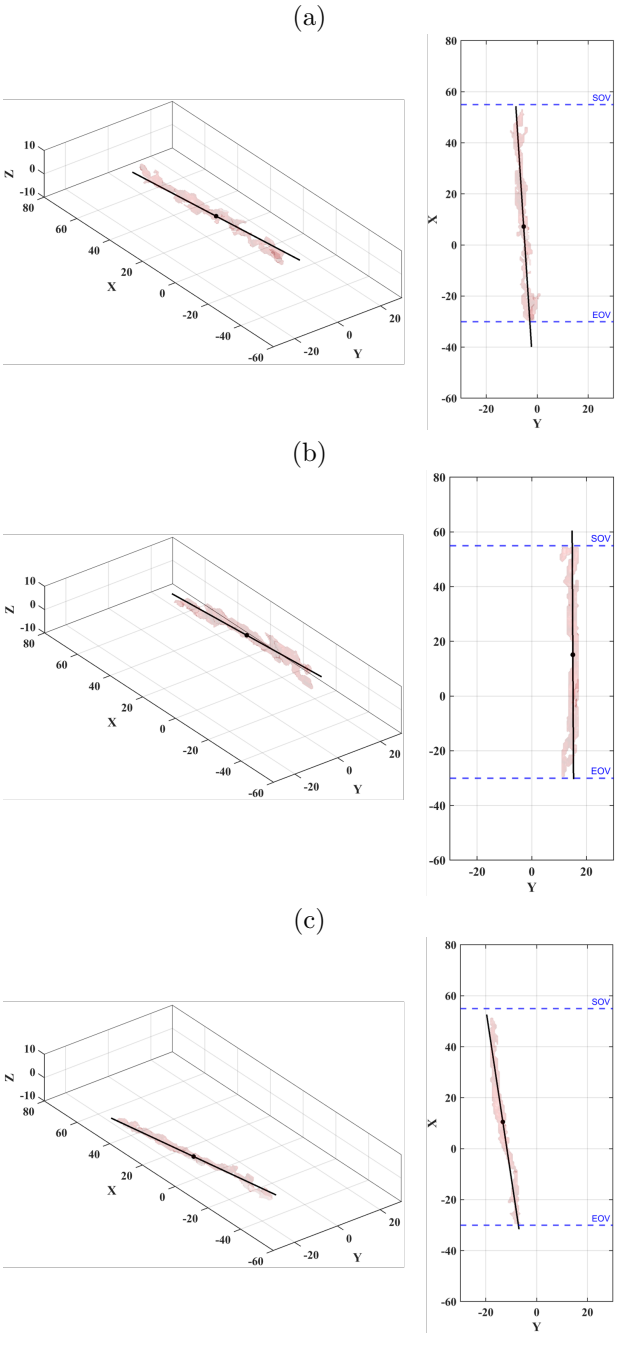

FIGURE S4. The 3-D views and the corresponding XY projections for three independent, instantaneous coherent vortical structures (a−c) visualized within volume P3 using isosurface threshold of $|\omega| = 40\ \mathrm{s}^{-1}$ ($|\omega|/S_{\max} = 0.78$). The centroid and the major principal axis of the equivalent ellipsoid fitted to structure are indicated by the black dot and the solid line. The length of the line corresponds to the major-axis length L of the ellipsoid. SOV and EOV denote the start and end of the volume in region P3. The XYZ coordinate system shown is local to region P3 as used in the spatial calibration. The axis X here corresponds to axis $-x$ shown in main Figure 1 with a streamwise shift, whereas axes Y, Z coincide with y, z. The origin [0,0,0] in XYZ coordinate corresponds to [296,0,0] mm in the xyz coordinate system shown in Fig. 1.

S5. Mean Velocity & Vorticity Fields

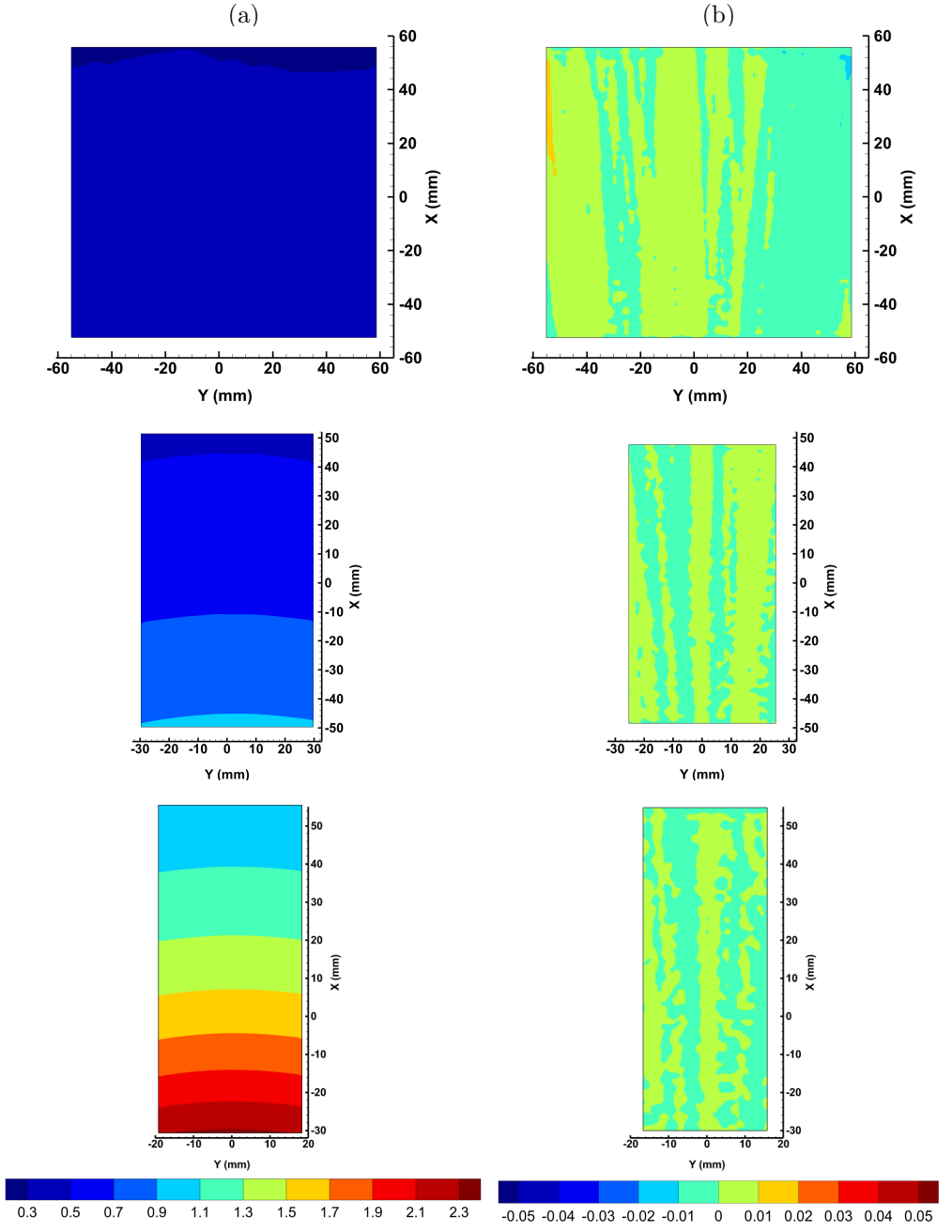

FIGURE S5. Contours of the time-averaged streamwise velocity $\langle U \rangle$ (m/s) (a) and the normalized $z-$vorticity $\langle \omega_z \rangle \,/\, |\boldsymbol{\omega}|_{max}$ (b) in the mid $X-Y$ plane of the measurement volumes P1, P2 & P3. Here, we set $|\boldsymbol{\omega}|_{max}$ = 80 s^{-1} as indicating approximately the maximum core strength that occurs near the exit of the contraction. The $X-Y$ coordinate system shown in the figure is used for calibration and is local to the measurement locations. Here the origin [0,0] shown in P1 corresponds to [55,0] in the $x-y$ coordinates. Similarly the origin [0,0] in P2 corresponds to [x =173,y =0] and in P3 corresponds to [x =296,y =0].

S6. Coherent Structures at low Re_λ

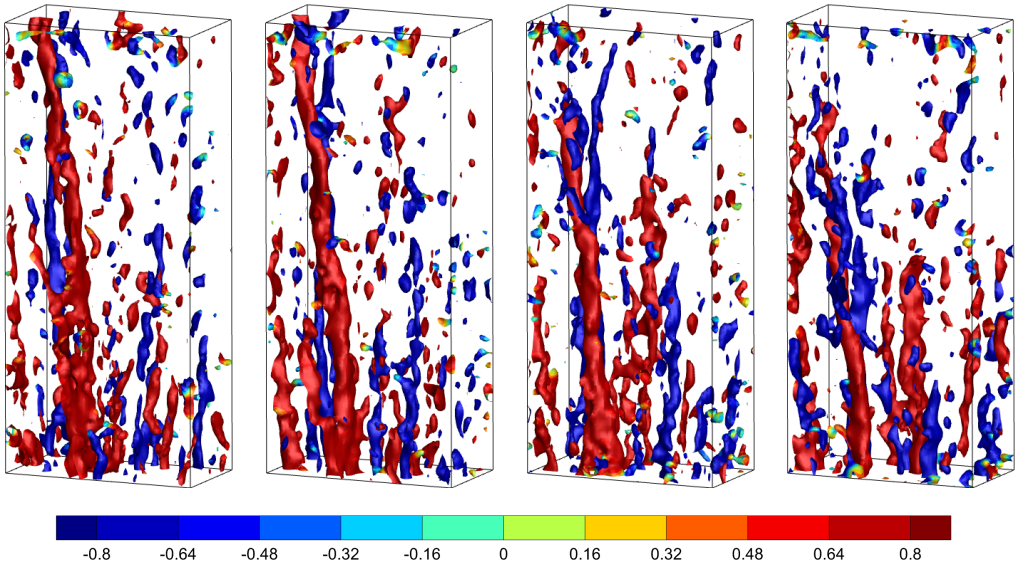

FIGURE S6. The time evolution of coherent structures at the lower $Re_\lambda \approx 110$, in Set II. Structures are visualized in region P3 by iso-surfaces $|\omega|/S_{\max} = 0.78$ and colored based on the rotation about the vertical axis. Refer to Figure 4 for more details.

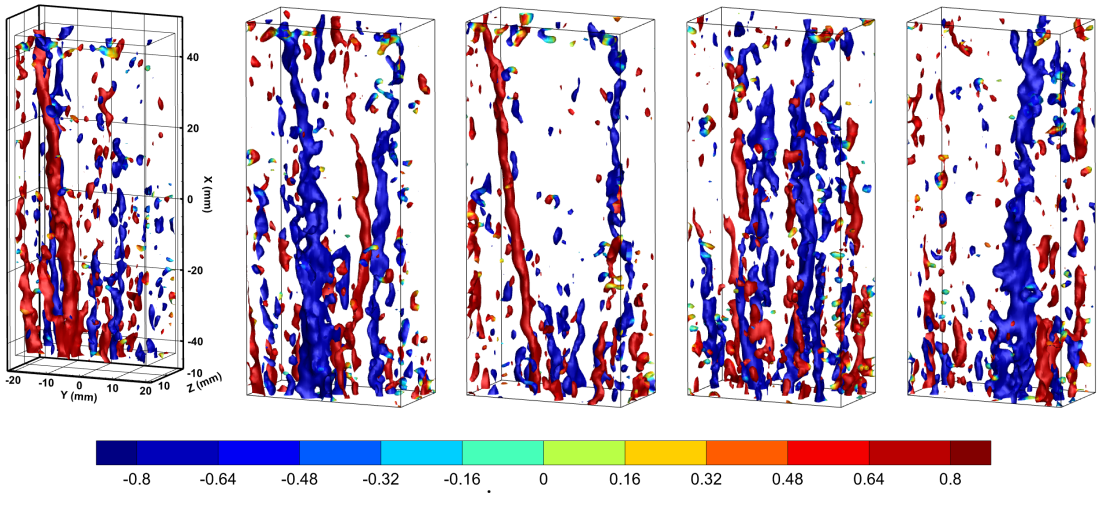

FIGURE S7. The independent coherent vortical structures at $Re_\lambda \approx 110$ that appear at different instants, one from each of the five different experimental runs. Structures are visualized in region P3 by iso-surfaces $|\omega|/S_{\max} = 0.78$ and colored based on their rotation about the vertical axis.

S7. Measurement uncertainty and convergence

We present the uncertainty of particle tracks and their velocities, calculated using DaVis 10.2 software from LaVision. The estimation is based on the method of Janke &

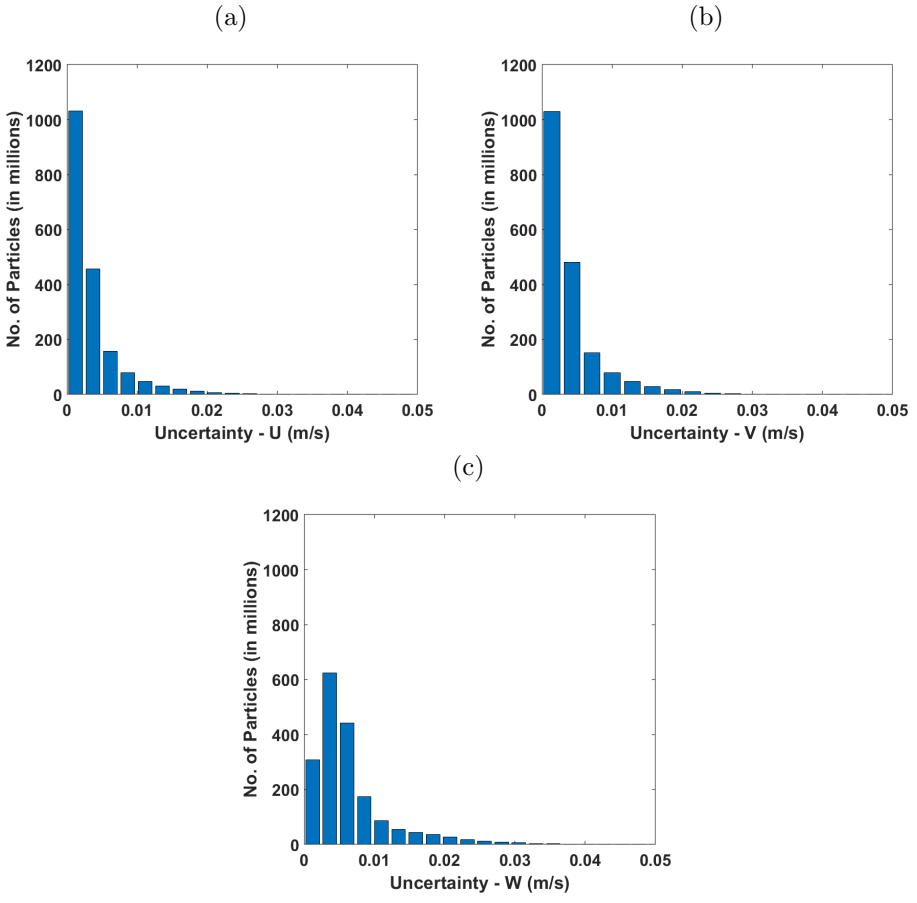

FIGURE S8. The bar chart of uncertainty in the particle velocity components: u (a), v (b) and w (c), predicted using the particle trajectories in the measurement region P1. These computations are made over billion particles in DaVis V10.2.

Michaelis (2021) wherein they estimate the uncertainty in particle position and velocity by calculating confidence bands of the polynomial fits of the particle trajectories. Figure S8 shows the bar chart of the uncertainty in particle velocity estimated with over a billion particles in 20,000 volumes.

We compute the standard deviation of this uncertainty distribution for the inlet and outlet measurement locations P1 & P3. The standard deviation for each location is presented below as a fraction of the respective mean streamwise velocity at location's inlet.

(1) In region P1, the uncertainty in u, v & w are 1.4%, 1.5% & 2.0% respectively;
(2) In region P3, they are 0.8%, 0.8% & 1.8%.

These values are within the accuracy limits reported by Sciacchitano *et al.* (2021). They performed a comparative study of different LPT algorithms which included DaVis and report that the accuracy of the algorithms in predicting particle velocities was between $0.3 - 2.5\%$ when the particle concentration was in the range, $0.005{-}0.016$ particles-per-pixel (ppp).

The uncertainty in the particle positions in the x, y & z directions was computed to be 0.07, 0.07 and 0.1 pixels respectively. This also falls inline with the uncertainty reported in the literature (Rowin & Ghaemi 2019; Schröder & Schanz 2023). For example Rowin & Ghaemi (2019) used LPT methods to investigate wall turbulent flow near super hydrophobic surfaces using LPT implemented in Davis 8.4., wherein they reported in-plane & out-of-plane position accuracy of 0.1 and 0.2 pixels respectively.

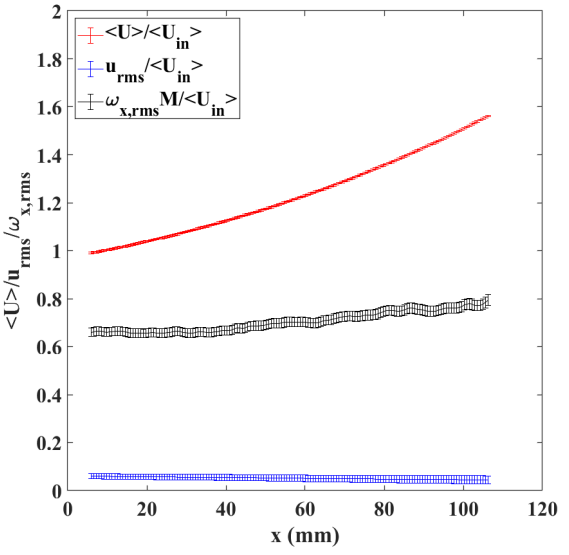

FIGURE S9. Convergence error bars in measurement region P1, for the streamwise mean velocity, the streamwise r.m.s velocity and r.m.s of streamwise vorticity. The errors bars represent the 1-sigma deviation calculated using five independent realizations.

We compute the convergence error bars for the mean and r.m.s quantities in region P1 based on the five independent realizations of 20,000 volumes each. Figure S9 shows the convergence for mean and r.m.s of streamwise quantities with the corresponding convergence bars, which represent the r.m.s computed. The corresponding errors computed in region P1, for the various measured quantities are summarized below:

(1) Mean velocity: $\langle U \rangle$ is 0.2%;
(2) RMS velocity: u_{rms}, v_{rms}, w_{rms} are 6.5%, 6.6%, & 6.1% respectively; and
(3) RMS vorticity: $\omega_{x,rms}$, $\omega_{y,rms}$, $\omega_{z,rms}$ are 2.8%, 2.8%, and 2.6% respectively.

REFERENCES

JANKE, T. & MICHAELIS, D. 2021 Uncertainty quantification for ptv/lpt data and adaptive track filtering. *14th International Symposium on Particle Image Velocimetry – ISPIV 2021* .

ROWIN, W. A. & GHAEMI, S. 2019 Streamwise and spanwise slip over a superhydrophobic surface. *J. of Fluid Mech.* **870**, 1127–1157.

SCHRÖDER, A. & SCHANZ, D. 2023 3d lagrangian particle tracking in fluid mechanics. *Annu. Rev. Fluid Mech.* **55**, 511–540.

SCIACCHITANO, A., LECLAIRE, B. & SCHRÖDER, A. 2021 Main results of the first lagrangian particle tracking challenge. *14th International Symposium on Particle Image Velocimetry – ISPIV 2021* .